Electric-field-dependent bimodal distribution functions for electrons in argon, xenon, and krypton owing to the Ramsauer-Townsend minima in the electron-atom momentum-transfer cross sections

Bernard Shizgal ⬤

Institute of Applied Mathematics, University of British Columbia, Vancouver, British Columbia, Canada V6T 1Z4

This paper considers solutions of the linear Fokker-Planck equation for the steady velocity distribution functions of electrons dilutely dispersed in an excess of either argon, xenon, or krypton. Owing to the large Ramsauer-Townsend minima in the electron-atom momentum-transfer cross sections for these atoms, the steady electron distribution, often referred to as the Davydov distribution, exhibits a bimodal distribution which varies dramatically with the strength of the external electric field. This effect provides a unique verification of the location and shape of the Ramsauer-Townsend minima in the cross sections. It is anticipated that current experimental techniques that probe the details of nonequilibrium electron distributions will verify the results reported in this paper. In addition, these nonequilibrium, non-Maxwellian distributions cannot be rationalized in terms of either the Gibbs-Boltzmann entropy nor the Tsallis nonextensive entropy.

I. INTRODUCTION

The statistical mechanics of electrons dilutely dispersed in a heat bath of atoms and subjected to an external electric field has provided a rich set of phenomena. Under the influence of an external electric field, the electron distribution function departs from a Maxwellian and is referred to as a Davydov distribution [1]. The effects reported include the transient negative mobility of electrons in xenon [2–5] and the negative differential conductivity of electrons in He-Xe and He-Kr mixtures [6–9], and other systems notably molecular [10–12]. The relaxation of electrons from some initial distribution to a steady nonequilibrium distribution referred to as the Davydov distribution [1] has been studied in detail [12–16]. The investigation of the charged particle transport in the inert gases has important applications [17] in numerous fields. The analyses of the nonequilibrium distributions associated with these phenomena are based on the Fokker-Planck equation for the electron energy distribution function.

The present work is directed towards a study of the bimodal nature of the distributions of electrons in the heavier inert gases, Ar, Kr, and Xe, over a narrow range of external electric field values. The bimodality arises form the Ramsauer-Townsend minima in the electron-atom momentum-transfer cross sections for these atoms. This effect does not appear to have been previously studied in depth except for the work of Makabe and Mori [18] and Zigman [19]. A bimodal particle velocity distribution has also been observed in granular flows [20], in laser-cooled atoms [21,22], and laser ablation [23]. The results reported here could potentially be used to better parametrize the electron-atom cross sections.

In Sec. II, the Fokker-Planck equation that describes the time evolution of the electron distribution is presented. This has been employed extensively in the study of the relaxation of electrons in the inert gases as well as for several molecular systems including electron attachment [24–27]. In this paper, the steady solution is considered in detail and the time-dependent approach to the bimodal distributions will be reported in a subsequent publication.

In Sec. III, the details of the bimodal distributions are presented for the three noble gases (Ar, Kr, and Xe) and the origin of the bimodality identified. It arises from the Ramsauer-Townsend minima in the momentum-transfer cross sections for these atoms. A comparison of the effect in the different atomic systems is presented as well as the use of different electron-atom momentum-transfer cross sections reported in the literature.

In Sec. IV, a review of numerous collision cross-section data for electron-atom systems is provided with special emphasis on the minima in the cross sections known as the Ramsauer-Townsend minimum. The data reviewed are not entirely consistent and there is no effort made to reconcile the differences. The purpose is to use these data as model cross sections to illustrate the manner in which the Ramsauer-Townsend minima dictate the bimodal features of the electron distributions for a small range of electric fields. These features of the electron distribution functions are discussed.

In Sec. V, the physical origin of the bimodal form of the distribution functions is demonstrated from the Pearson differential equation [28,29] that defines the stationary distributions. A comparison between electrons in Kr with electrons in Xe is presented. A summary of the results is also provided with the suggestion that the effects reported here could potentially be observed experimentally based on historical measurements of non-Maxwellian distributions in different physical systems.

II. FOKKER-PLANCK EQUATION FOR ELECTRONS IN AN ATOMIC MODERATOR

We consider an ensemble of electrons dilutely dispersed in a large excess of an inert gas (argon, krypton, or xenon) at

022805-1

temperature T_b, density n, and subject to an external electric field of strength E. With the definitions of the reduced electron speed, $x = v\sqrt{m/2k_BT_b}$, where m denotes the electron mass and k_B the Boltzmann constant, the electron distribution $f(x, t)$ is given by the Fokker-Planck equation [2,3],

$$\frac{\partial f(x,t)}{\partial t} = \frac{1}{x^2}\frac{\partial}{\partial x}\left[2x^4\hat{\sigma}(x)f + x^2 B(x)\frac{\partial f}{\partial x}\right], \qquad (1)$$

where

$$B(x) = x\hat{\sigma}(x) + \frac{\alpha^2}{x\hat{\sigma}(x)}, \qquad (2)$$

and $\hat{\sigma}(x) = \sigma(x)/\sigma_0$, where σ_0 is a convenient hard-sphere cross section generally chosen as 1 Å^2. The electric field strength parameter α is defined by

$$\alpha^2 = \frac{M}{6m}\left[\frac{eE}{n\sigma_0 k_B T_b}\right]^2, \qquad (3)$$

where e is the electron charge. The dimensionless time is defined as $t = t'/\tau$ where

$$\tau = \left[\frac{nm\sigma_0}{2M}\sqrt{\frac{2k_BT_b}{m}}\right]^{-1}. \qquad (4)$$

The steady-state distribution function is given by a Pearson differential equation [28,29] of the form

$$\frac{1}{f_{ss}}\frac{df_{ss}(x)}{dx} = -\frac{2x^2\sigma(x)}{B(x)}. \qquad (5)$$

The Fokker-Planck equation, Eq. (1), describes the evolution of the isotropic portion of the distribution function. The main objective in the present paper is the nature of the steady-state distributions versus the electric field strength for different electron-moderator cross sections. With Eq. (1), the steady nonequilibrium electron distribution arising from an interplay of the acceleration in a steady electric field and moderated by electron-atom collisions is given by

$$f_{ss}(x) = C \exp\left[-2\int_0^x \frac{y^2\sigma(y)}{B(y)}dy\right], \qquad (6)$$

where C is a normalization. The distribution function $f_{ss}(x)$ given by Eq. (6) is often referred to as the Davydov distribution [1,4].

III. ELECTRIC-FIELD-DEPENDENT BIMODAL ELECTRON DISTRIBUTIONS: A REFLECTION OF THE RAMSAUER-TOWNSEND MINIMA

There have been many determinations of the momentum-transfer cross sections for collisions of electrons with the inert gas atoms argon, krypton, and xenon with different techniques both experimental and theoretical as reported by numerous researchers[17,30–39]. A comparison of the energy variation of the momentum-transfer cross sections for electron collisions with argon, krypton, and xenon are shown in Figs. 1–3. The choice of the log-log plots enhances the Ramsauer minima in the cross sections which occur at very low energies. Kurokawa et al. [37] show a useful comparison of the linear and logarithmic representations of the cross sections. Some of the cross-section data shown are used in this work as models
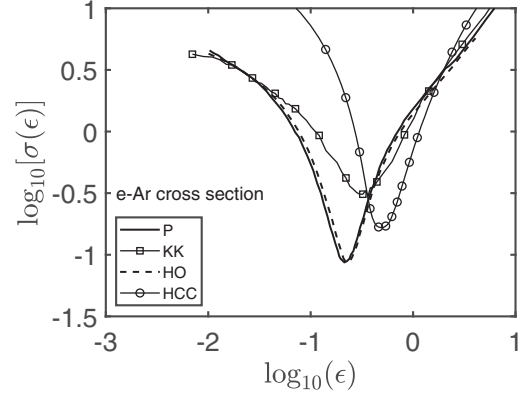

FIG. 1. Momentum transfer cross sections $\sigma(\epsilon)$ in Å^2 vs energy ϵ in electron volts for electron-argon collisions. The nearly coincident curves denoted by P (solid line) and HO (dashed line) are the cross sections reported by Pitchford et al. [35] and Haddad and O'Malley [31], respectively. The solid curve with square symbols denoted by KK is the momentum-transfer cross section reported by Kitajami et al. [37] whereas the solid curve with circles denoted by HCC is the cross section reported by Hunter, Carter, and Christophorou [34]. The log-log plot enhances the Ramsauer-Townsend minimum in the momentum-transfer cross section. The symbols are used to identify the momentum-transfer cross section and are not actual data.

of the actual cross sections although some may reflect the actual cross-section properties better than others. The results reported in this paper could be used together with additional experiments to better parametrize these cross-section data.

The steady electron distribution function for electrons in argon is given by Eq. (6) and shown in Fig. 4 as $F(x) = x^2 f(x)$. The added x^2 factor is responsible for the occurrence of the maxima in the distribution functions as it does for the Maxwellian. The electron distribution function is given by
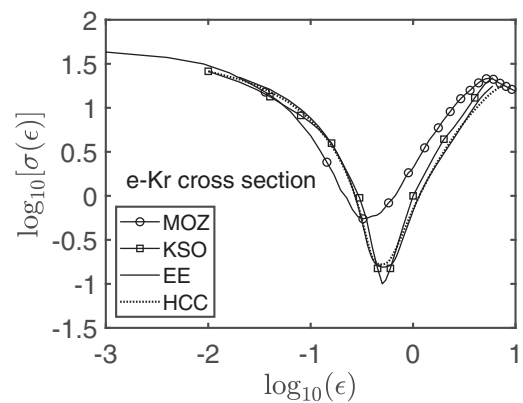

FIG. 2. Momentum transfer cross sections $\sigma(\epsilon)$ in Å^2 vs energy ϵ in electron volts for electron-krypton collisions as reported by Mozumder [30] (MOZ: solid line with circles), Koizumi, Shirakawa, and Ogawa [32] (KSO: solid line with squares), England and Elford [33] (EE: solid line), and Hunter, Carter, and Christophorou [34] (HCC: dotted line). The log-log plot enhances the Ramsauer-Townsend minimum in the momentum-transfer cross section. The symbols are used to identify the momentum-transfer cross section and are not actual data.
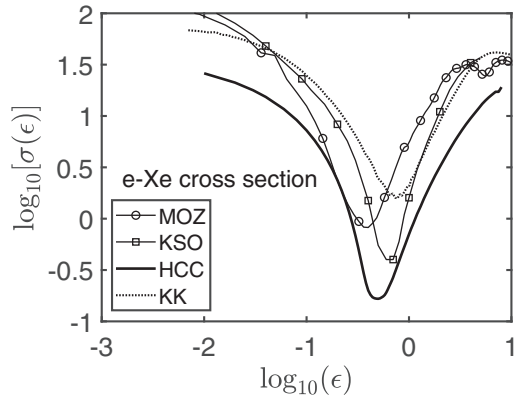
FIG. 3. Momentum transfer cross sections $\sigma(\epsilon)$ in Å^2 vs energy ϵ in electron volts for electron-xenon collisions. The solid curve with circles is the momentum-transfer cross section reported by Mozumder [30]. The solid curve with squares is the momentum-transfer cross section reported by Koizumi, Shirakawa, and Ogawa [32]. The heavy solid curve denoted by HCC is the momentum-transfer cross section reported by Hunter *et al.* [34]. The dotted line denoted by KK is the cross section reported by Kurokawa *et al.* [37]. The log-log plot enhances the Ramsauer-Townsend minimum in the momentum-transfer cross section. The symbols are used to identify the momentum-transfer cross section and are not actual data.

Eq. (6) and the integral is evaluated with a Simpson's rule. The analytic representation of the energy dependence of the e-Ar cross section [4] is given by

$$\sigma_{e\text{-Ar}}(\epsilon)$$
$$= (7.8945 - 30.3097\sqrt{\epsilon} + 30.7265\epsilon)/(1 + 5.1640\sqrt{\epsilon}), \tag{7}$$

with ϵ in eV and $\sigma(\epsilon)$ in Å^2, was reported in Ref. [4] in comparison with the cross-section data by Mozumder [30] and Haddad and O'Malley [31]. A typographical error in Eq. (7) in Ref. [4] is here corrected. The electric field strengths shown in the figure are chosen to show the change in the bimodal structure of the electron distribution function.
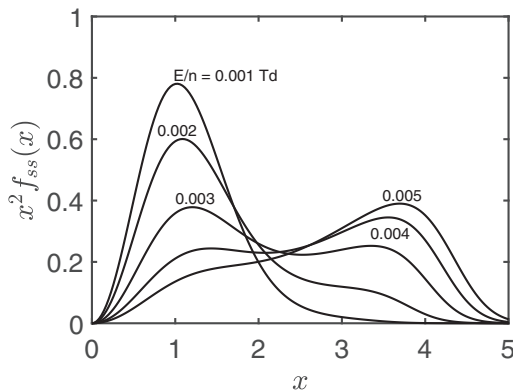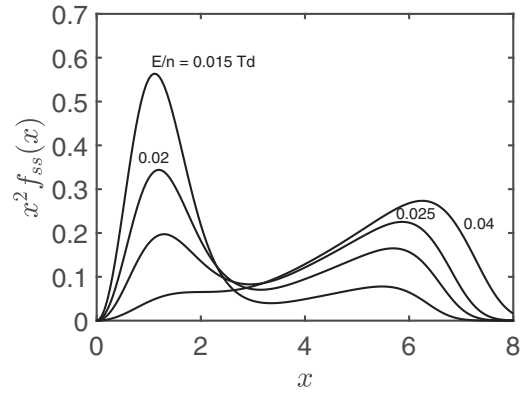

FIG. 5. Bimodal distributions of electrons in Kr for different electric field strengths E/n with the momentum-transfer cross section reported by Hunter, Carter, and Christophoru [34]; $x = \sqrt{mv^2/2k_BT_b}$, E/n in townsend, $\text{Td} = 10^{-17}$ V/cm^2; $T_b = 290$ K.

The steady electron distribution functions for electrons in krypton and xenon as given by Eq. (6) are shown in Figs. 5 and 6. The cross sections for e-Kr and e-Xe collisions are those reported by Hunter, Carter, and Christophorou [34]. As in Fig. 4, the electric field strengths shown in the figure are chosen so as to show the change in the bimodal structure of the electron distribution function. The range of electric fields in these cases is somewhat larger than for electron distributions in argon shown in Fig. 7. It would not be possible to report on the occurrence of these bimodal distributions for all 12 electron moderator cross sections summarized in Figs. 1–3. The bimodality arises owing to the Ramsauer-Townsend minima in the cross sections. The model cross sections summarized in Figs. 1–3 would yield different effects owing to the different positions of the minimum and the different depths.

In Fig. 7, the bimodal structure of the electron distribution for electrons in Kr is shown in the upper graphs and for electrons in Xe in the lower graph. The distribution functions shown with the solid curve are the results with the cross section reported by Hunter, Carter, and Christophorou [34] whereas the dashed curves are the results with the cross

FIG. 4. Bimodal distributions of electrons in argon for different electric field strengths E/n, $x = \sqrt{mv^2/2k_BT_b}$, E/n in townsend, $\text{Td} = 10^{-17}$ V/cm^2; $T_b = 290$ K. The e-Ar momentum-transfer cross section is the analytic fit reported in Ref. [26] as given by Eq. (7).
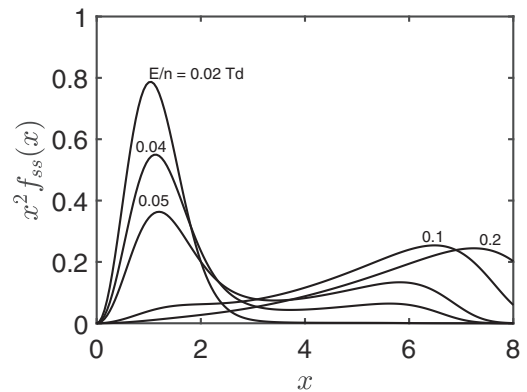

FIG. 6. Bimodal distributions of electrons in Xe for different electric field strengths with the momentum-transfer cross section reported by Hunter, Carter, and Christophoru [34]; $x = \sqrt{mv^2/2k_BT_b}$, E/n in townsend, $\text{Td} = 10^{-17}$ V/cm^2; $T_b = 290$ K.
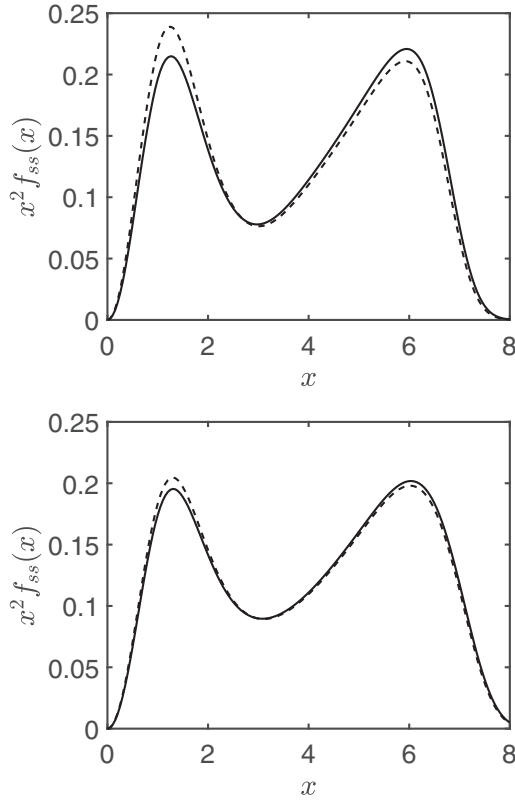
FIG. 7. Upper graph: Bimodal distributions of electrons in Kr, $E/n = 0.025$ Tn, with the momentum-transfer cross sections reported by England and Efford [33] (dashed line) and the momentum-transfer cross section reported by Hunter, Carter, and Christophorou [34] (solid line); $x = v/v_{\text{th}}$ with $v_{\text{th}} = \sqrt{2k_B T_b/m}$, E/n in townsend, Tn $= 10^{-17}$ V/cm^2; $T_b = 290$ K. Lower graph: Bimodal distributions of electrons in Xe, $E/n = 0.062$ Tn, with the momentum-transfer cross sections reported by England and Efford [33] (dashed line) and the momentum-transfer cross section reported by Hunter, Carter, and Christophorou [34] (solid line); $x = v/v_{\text{th}}$ with $v_{\text{th}} = \sqrt{2k_B T_b/m}$, E/n in townsend, Tn $= 10^{-17}$ V/cm^2; $T_b = 290$ K.

section reported by England and Efford [33]. For krypton, the two cross sections are nearly coincident as shown in Fig. 7 and the distributions are nearly coincident. The electric field strengths were chosen to have the maxima of the distribution functions at approximately the same values.

IV. PHYSICAL ORIGIN OF THE ELECTRON DISTRIBUTION BIMODALITY

The physical basis for the distribution function bimodality is due to the Ramsauer-Townsend minimum in the electron-inert atom momentum-transfer cross section. An important point is that the distribution functions shown in the figures are plotted as $x^2 f_{\text{ss}}(x)$ which exhibits the bimodality. The relationship with the cross sections can be determined with the defining equation for $f_{\text{ss}}(x)$ from the steady state of the Fokker-Planck equation, namely Eq. (1), and given by Eq. (6).

The relationship between the bimodal distribution functions $x^2 f_{\text{ss}}(x)$, in Figs. 4–7 and the Ramsauer-Townsend minima in the momentum-transfer cross section can be explained with the Pearson differential equation [28,29], Eq. (5),

for the steady distributions, that is,

$$\frac{1}{f_{\text{ss}}}\frac{df_{\text{ss}}}{dx} = -\frac{2x^2\hat{\sigma}}{\left(x\hat{\sigma} + \frac{\alpha^2}{x\hat{\sigma}}\right)}. \tag{8}$$

The bimodality of $F(x) = x^2 f_{\text{ss}}(x)$ as depending on E/n and the RT minimum in $\hat{\sigma}(x)$ is given by

$$\begin{aligned}\frac{1}{F}\frac{dF}{dx} &= \frac{1}{x^2 f_{\text{ss}}}\left(2x f_{\text{ss}} + x^2 \frac{df_{\text{ss}}}{dx}\right) \\ &= \frac{2}{x}\left(1 - \frac{x^3\hat{\sigma}}{x\hat{\sigma} + \frac{\alpha^2}{x\hat{\sigma}}}\right) \\ &= \frac{2}{x}\left(\frac{x\hat{\sigma} + \frac{\alpha^2}{x\hat{\sigma}} - x^3\hat{\sigma}}{x\hat{\sigma} + \frac{\alpha^2}{x\hat{\sigma}}}\right). \end{aligned} \tag{9}$$

Thus, the maxima in the distribution function $F(x)$ are defined by

$$x^2\hat{\sigma}^2 + \alpha^2 - x^4\hat{\sigma}^2 = 0, \tag{10}$$

or equivalently

$$\hat{\sigma}^2 = \frac{\alpha^2}{x^2(x^2 - 1)}. \tag{11}$$

Thus there can be several roots to Eq. (11) as dependent on the electric field strength E/n which defines α.

Figure 8 verifies the bimodal distribution functions as arising from the Ransauer-Townsend minima in the momentum-transfer cross section. The upper figure shows the bimodal distribution for electrons in Kr with the cross section reported by Hunter, Carter, and Christophoru [34] and $E/n = 0.015$ Tn. The solid circles identify the minimum and the outermost maximum in the bimodal distribution function. The lower graph shows the analysis based on Eq. (11) with the intersection of the dashed and solid curves identifying the minimum and maximum in the distribution. This would not occur if not for the minimum in the momentum-transfer cross Sec. IV.

Figure 9 verifies the bimodal distribution functions as arising from the Ransauer-Townsend minima in the momentum-transfer cross section. The upper figure shows the bimodal distribution for electrons in Xe with the cross section reported by Hunter, Carter, and Christophoru [34] and $E/n = 0.055$ Tn. The solid circles identify the minimum and the outermost maximum in the bimodal distribution function. The lower graph shows the analysis based on Eq. (11) with the intersection of the dashed and solid curves identifying the minimum and maximum in the distribution. This would not occur if not for the minimum in the momentum-transfer cross section.

The results in Figs. 8 and 9 could potentially be used to *invert* measurements of the bimodal distributions to extract the momentum-transfer cross sections. The minimum and the maximum in the upper graph of Figs. 8 and 9 identify two values of the momentum-transfer cross section. With a change in the electric field strength the minimum and the maximum move in reduced speed x as shown in Figs. 4–6 and in this way scan the momentum-transfer cross section. Ultimately, it may be possible to extract the momentum transfer cross section for a range of relative energies.
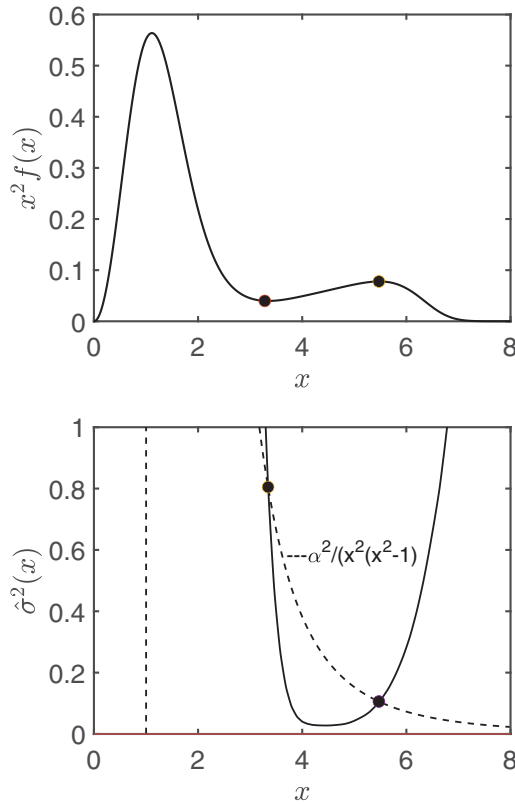
FIG. 8. Upper graph: The solid line is the bimodal distribution of electrons in Kr, $E/n = 0.015$ Tn, with the momentum-transfer cross sections reported by Hunter, Carter, and Christophorou [34]; $x = v/v_{\text{th}}$ with $v_{\text{th}} = \sqrt{2k_B T_b/m}$, E/n in townsend, Tn $= 10^{-17}$ V/cm^2; $T_b = 290$ K. The solid circles identify the outermost extrema in the bimodal distribution. Lower graph: Analysis of the bimodal distribution based on Eq. (11). The solid curve is $\hat{\sigma}^2(x)$ with the Ramsauer-Townsend minimum and the dashed curve is as noted.
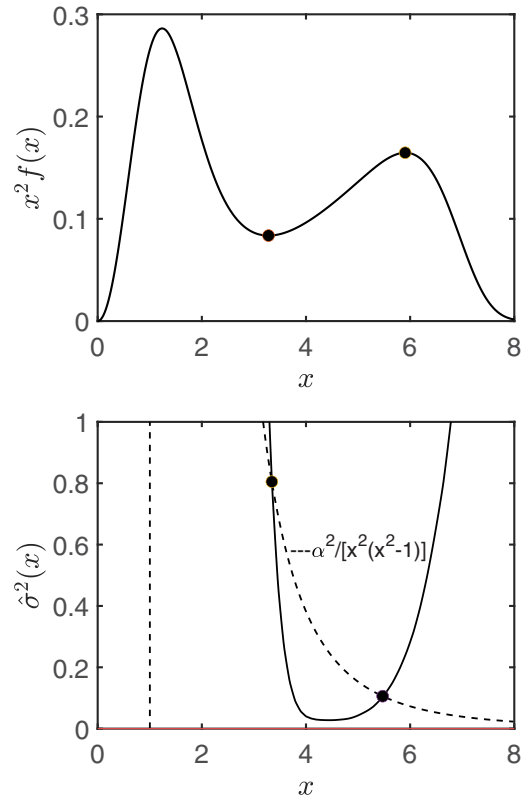

FIG. 9. Upper graph: The solid line is the bimodal distribution of electrons in Xe, $E/n = 0.055$ Tn, with the momentum-transfer cross sections reported by Hunter, Carter, and Christophorou [34]; $x = v/v_{\text{th}}$ with $v_{\text{th}} = \sqrt{2k_B T_b/m}$, E/n in townsend, Tn $= 10^{-17}$ V/cm^2; $T_b = 290$ K. The solid circles identify the outermost extrema in the bimodal distribution. Lower graph: Analysis of the bimodal distribution based on Eq. (11). The solid curve is $\hat{\sigma}^2(x)$ with the Ramsauer-Townsend minimum and the dashed curve is as noted.

V. SUMMARY

In this paper, the bimodal nature of the electron distribution function in different inert gases that act as a heat bath was demonstrated as arising from the Ramsauer-Townsend minima in the electron-atom momentum-transfer cross sections. The range of the electric field strengths for which the bimodality occurs is narrow and occurs for low E/n values as dependent on the moderator. The origin of the bimodal structure was reported in Sec. IV.

There have been numerous reportings of measurements of non-Maxwellian features for electrons and ions in different physical situations. In particular, one should note the work reported by Milder *et al.* [40] on the measurement of the electron distribution functions during laser heating. Takahashi, Charles, and Boswell [41] report measurements of the electron energy distribution functions in a double layer. Blackwell and Chen [42] report on the measurements of the electron energy distribution in a plasma. Lohmann and Weigold [43] reported a direct measurement of the electron distribution in atomic hydrogen. Although these physical situations differ from the systems reported in this paper it may be possible to adapt these and similar diagnostics of electron distributions so as to measure the bimodal distributions [44–50].

[1] G. H. Wannier, Derivation of the Davydov distribution from the Boltzmann equation, Am. J. Phys. **39**, 281 (1971).

[2] D. R. A. McMahon and B. Shizgal, Hot-electron zero-field mobility and diffusion in rare-gas moderators, Phys. Rev. A **31**, 1894 (1985).

[3] B. Shizgal and D. R. A. McMahon, Electric field dependence of transient electron transport properties in rare gas moderators, Phys. Rev. A **32**, 3669 (1985).

[4] K. Leung, B. D. Shizgal, and H. Chen, The quadrature discretization method (QDM) in comparison with other numerical methods of solution of the Fokker-Planck equation for electron thermalization, J. Math. Chem. **24**, 291 (1998).

[5] J. M. Warman, U. Sowada, and M. P. De Hass, Transient negative mobility of hot electrons in gaseous xenon, Phys. Rev. A **31**, 1974 (1985).

[6] B. Shizgal, Negative differential conductivity of electrons in He-Xe and He-Kr mixtures, Chem. Phys. **147**, 271 (1990).

[7] N. L. Aleksandrov, N. A. Dyatko, I. V. Kochentov, A. P. Nepartovich, and D. Lo, Negative differential conductivity of electrons in pure rare gases, Phys. Rev. E **53**, 2730 (1996).

[8] R. E. Robson, Z. Lj. Petrović, Z. M. Raspopović, and D. Loffhagen, Negative absolute electron mobility, Joule cooling and the second law, J. Chem. Phys. **119**, 11249 (2003).

[9] Z. Lj. Petrovic, R. W. Crompton, and G. N. Haddad, Model calculations of negative differential conductivity in gases, Aust. J. Phys. **37**, 23 (1984).

[10] S. Dujko, Z. M. Raspopović, Z. Lj. Petrović and T. Makabe, Negative mobilities of electrons in radio frequency fields, IEEE Trans. Plasma Sci. **31**, 711 (2003).

[11] S. B. Vrhovac and Z. Lj. Petrović, Momentum transfer theory of nonconservative charged particle transport in mixtures of gases: General equations and negative differential conductivity, Phys. Rev. E **53**, 4012 (1996).

[12] R. D. White, S. Dujko, K. F. Ness, R. E. Robson, Z. Raspopović, and Z. Lj. Petrović, On the existence of transiently negative diffusion coefficients for electrons in gases in $E \times B$ fields, J. Phys. D: Appl. Phys. **41**, 025206 (2008).

[13] B. Shizgal and D. R. A. McMahon, Electron distribution functions and thermalization times in inert gas moderators, J. Phys. Chem. **88**, 4854 (1984).

[14] R. Sospedra-Alfonso and B. D. Shizgal, Killback-Leibler entropy in the electron distribution shape relaxation for electron-atom thermalization, Phys. Rev. E **84**, 041202 (2011).

[15] R. Sospedra-Alfonso and B. D. Shizgal, Energy and shape relaxation in binary atomic systems with realistic quantum cross sections, J. Chem. Phys. **139**, 044113 (2013).

[16] I. K. Bronić and M. Kimura, Electron thermalization in rare gases and their mixtures, J. Chem. Phys. **104**, 8973 (1996).

[17] I. Simonović, D. Bossnjaković, Z. Lj. Petrović, R. D. White, and S. Dujko, Third-order transport coefficient tensor of electron swarms in noble gases, Eur. Phys. J. D **74**, 63 (2020).

[18] T. Makabe and T. Mori, Variations in electron transport in argon with temperature near the Ramsauer-Townsend minimum, J. Phys. D: Appl. Phys. **15**, 1395 (1982).

[19] V. Žigman, Influence of the Ramsauer—Townsend minimum on the electron energy distribution function and electron transport in xenon, J. Plasma Phys. **72**, 525 (2006).

[20] B. Zhao and J. Wang, Topography analysis of particle velocity distribution function in gas-solid flow, Chem. Eng. Sci. **197**, 69 (2019).

[21] Y. Shevy, D. S. Weiss, P. J. Ungar, and S. Chiu, Bimodal Speed Distribution in Laser-Cooled Atoms, Phys. Rev. Lett. **62**, 1118 (1989).

[22] C. M. Dion, S. Jonsell, A. Kastberg, and P. Sjölund, Bimodal momentum distributions in laser cooled atoms in optical lattices, Phys. Rev. A **93**, 053416 (2016).

[23] J. Maul, S. Karpuk, and G. Huber, Bimodal velocity distribution of atoms released from nanosecond ultraviolet laser ablation, Phys. Rev. B **71**, 045428 (2005).

[24] B. D. Shizgal and K. Kowari, Electron attachment kinetics coupled to electron thermalization in SF_6/Ar mixtures, J. Phys. D: Appl. Phys. **35**, 973 (2002).

[25] B. Shizgal, A uniform WKB analysis of the coupling of electron attachment and thermalization in gases, J. Phys. B: At., Mol. Opt. Phys. **24**, 2909 (1991).

[26] K. Kowari, K. Leung, and B. D. Shizgal, The coupling of electron thermalization and electron attachment in CCl_4/Ar and CCl_4/Ne mixtures, J. Chem. Phys. **108**, 1587 (1998).

[27] K. Wnorowski, J. Wnorowska, B. Michalczuk, A. Jówko, and W. Barszczewska, Thermal electron attachment to chlorinated alkenes in the gas phase, Chem. Phys. Lett. **667**, 272 (2017).

[28] B. D. Shizgal, Suprathermal particle distributions in space physics: Kappa distributions and entropy, Astrophys. Space Sci. **312**, 227 (2007).

[29] B. Shizgal, The use of the Pearson differential equation to test energetic distributions in space physics as Kappa distributions; implication for Tsallis nonextensive entropy: II, Astrophys. Space Sci. **367**, 7 (2022).

[30] A. Mozumder, Electron thermalization in gases. II. Neon, argon, krypton, and xenon, J. Chem. Phys. **72**, 6289 (1980).

[31] G. N. Haddad and T. F. O'Malley, Scattering cross sections in argon from electron transport Parameters, Aust. J. Phys. **35**, 35 (1982).

[32] T. Koizumi, E. Shirakawa, and I. Ogawa, Momentum transfer cross sections for low-energy electrons in krypton and xenon from characteristic energies, J. Phys. B: At. Mol. Phys. **19**, 2331 (1986).

[33] J. P. England and M. T. Elford, Momentum transfer cross section for electrons in Krypton derived from measurements of the drift velocity in H_2-Kr muxtures, Aust. J. Phys. **41**, 701 (1988).

[34] S. R. Hunter, J. G. Carter, and L. G. Christophorou, Low-energy electron drift and scattering in krypton and xenon, Phys. Rev. A **38**, 5539 (1988).

[35] L. C. Pitchford, L. L. Alves, K. Bartschat, S. F. Biagi, M. C. Bordage, A. V. Phelps, C. M. Ferreira, G. J. M. Hagelaar, W. L. Morgan, S. Pancheshnyi *et al.*, Comparisons of sets of electron-neutral scattering cross sections and swarm parameters in noble gases: I. Argon, J. Phys. D: Appl. Phys. **46**, 334001 (2013).

[36] H. B. Milloy, R. W. Crompton, J. A. Rees, and A. G. Robertson, The momentum transfer cross section for electrons in argon in the energy range 0–4 eV, Aust. J. Phys. **30**, 61 (1977).

[37] M. Kurokawa, M. Kitajima, K. Toyoshima, T. Kishino, T. Odagiri, H. Kato, M. Hoshino, H. Tanaka, and K. Ito, High-resolution total-cross-section measurements for electron scattering from Ar, Kr, and Xe, employing a threshold photoelectron source, Phys. Rev. A **84**, 062717 (2011).

[38] R. P. McEachran and A. D. Stauffer, Viscosity cross sections for the heavy noble gases, Eur. Phys. J. D **69**, 106 (2015).

[39] S. Rosmej, H. Reinholz, and G. Röpke, Contribution of electron-atom collisions to plasma conductivity of noble gases, Phys. Rev. E **95**, 063208 (2017).

[40] A. L. Milder, J. Katz, R. Boni, J. P. Palastro, M. Sherlock, W. Rozmus, and D. H. Froula, Measurements of Non-Maxwellian Electron Distribution Functions and Their Effect on Laser Heating, Phys. Rev. Lett. **127**, 015001 (2021).

[41] K. Takahashi, C. Charles, R. W. Boswell, T. Kaneko, and R. Hatakeyama, Measurement of the energy distribution of trapped and free electrons in a current-free double layer, Phys. Plasmas **14**, 114503 (2007).

[42] D. D. Blackwell and F. F. Chen, Time-resolved measurements of the electron energy distribution function in a helicon plasma, Plasma Sources Sci. Technol. **10**, 226 (2001).

[43] B. Lohmann and E. Weigold, Direct measurement of the electron momentum probability distribution in atomic hydrogen, Phys. Lett. A **86**, 139 (1981).

[44] D. R. A. McMahon, K. Ness, and B. Shizgal, Electric field dependence of transient electron longitudinal and transverse diffusion coefficients in rare-gas moderators, J. Phys. B: At. Mol. Phys. **19**, 2759 (1986).

[45] E. Suzuki and Y. Hatano, Electron thermalization processes in rare gases with the Ramsauer minimum, J. Chem. Phys. **84**, 4915 (1986).

[46] B. Shizgal, D. R. A. McMahon, and L. A. Viehland, International Journal of Radiation Applications and Instrumentation. Part C. Radiation Physics and Chemistry, Radiat. Phys. Chem. **34**, 35 (1989).

[47] A. I. Shchedrin, A. V. Ryabtsev, and D. Lo, Absolute negative conductivity in Xe/Cs mixture under photoionization conditions, J. Phys. B: At. Mol. Phys. **29**, 915 (1996).

[48] D. Blake and R. E. Robson, Negative differential conductivity in gases. The "true origin", J. Phys. Soc. Jpn. **70**, 3556 (2001).

[49] W. Zhang and B. D. Shizgal, Fokker-Planck equation for Coulomb relaxation and wave-particle diffusion: Spectral solution and the stability of the Kappa distribution to Coulomb collisions, Phys. Rev. E **102**, 062103 (2020).

[50] K. Kowari, L. Demeio, and B. Shizgal, Electron degradation and thermalization in CH_4 gas, J. Chem. Phys. **97**, 2061 (1992).